Molecular-Based Magnetism in Bimetallic Two-Dimensional Oxalate-Bridged Networks. An X-ray and Neutron Diffraction Study

René Pellaux,[†] Helmut W. Schmalle,[†] Reto Huber,[†] Peter Fischer,[‡] Thomas Hauss,[§] Bachir Ouladdiaf,[||] and Silvio Decurtins*,[†]

Institut für Anorganische Chemie, Universität Zürich, Winterthurerstrasse 190, CH-8057 Zürich, Switzerland, Laboratorium für Neutronenstreuung, Eidgenössische Technische Hochschule Zürich & Paul Scherrer Institut, CH-5232 Villigen PSI, Switzerland, Hahn-Meitner-Institut, Abteilung für Neutronenstreuung, Glienickerstrasse 100, D-1000 Berlin 39, Germany, and Institut Laue-Langevin, BP 156, F-38042 Grenoble Cedex 9, France

Received July 17, 1996[⊗]

Bimetallic, oxalate-bridged compounds with bi- and trivalent transition metals comprise a class of layered materials which express a large variety in their molecular-based magnetic behavior. Because of this, the availability of the corresponding single-crystal structural data is essential to the successful interpretation of the experimental magnetic results. We report in this paper the crystal structure and magnetic properties of the ferromagnetic compound $\{[N(n\text{-}C_3H_7)_4][Mn^{II}Cr^{III}(C_2O_4)_3]\}_n$ (**1**), the crystal structure of the antiferromagnetic compound $\{[N(n\text{-}C_4H_9)_4][Mn^{II}Fe^{III}(C_2O_4)_3]\}_n$ (**2**), and the results of a neutron diffraction study of a polycrystalline sample of the ferromagnetic compound $\{[P(C_6D_5)_4][Mn^{II}Cr^{III}(C_2O_4)_3]\}_n$ (**3**). Crystal data: **1**, rhombohedral, *R*3*c*, $a = 9.363(3)$ Å, $c = 49.207(27)$ Å, $Z = 6$; **2**, hexagonal, $P6_3$, $a = 9.482(2)$ Å, $c = 17.827(8)$ Å, $Z = 2$. The structures consist of anionic, two-dimensional, honeycomb networks formed by the oxalate-bridged metal ions, interleaved by the templating cations. Single-crystal field dependent magnetization measurements as well as elastic neutron scattering experiments on the manganese(II)−chromium(III) samples show the existence of long-range ferromagnetic ordering behavior below $T_c = 6$ K. The magnetic structure corresponds to an alignment of the spins perpendicular to the network layers. In contrast, the manganese(II)−iron(III) compound expresses a two-dimensional antiferromagnetic ordering.

Introduction

In the field of molecular-based magnetism,[1] structurally two-dimensional (2D) bimetallic oxalate-bridged networks have attracted increasing interest in recent years.[2−11] This class of compounds shows a general stoichiometry of the type $\{[A][M^{II}M'^{III}(ox)_3]\}_n$, where A^+ is a monopositive cation, $A^+ = [XR_4]^+$ (X = N, P; R = *n*-propyl, *n*-butyl, *n*-pentyl, phenyl), and ox^{2-} is $(C_2O_4)^{2-}$. The most notable feature of these materials is that a wide variety of metal ion combinations can be incorporated into the same basic structure consisting of infinitely extended layers of oxalate-bridged metal ions, exhibiting hexagonal symmetry and being separated by the templating counterions A^+. Since the ambidentate oxalate ions act as mediators for magnetic exchange interactions between the transition-metal centers, short-range and long-range magnetic ordering behavior may occur, and consequently, from this molecular class of compounds emerge materials with distinct magnetic properties. As a matter of fact, within the series $\{[N(n\text{-}C_4H_9)_4][M^{II}Cr^{III}(ox)_3]\}_n$, M^{II} = Mn, Fe, Co, Ni, Cu, which has been shown to be structurally two-dimensional,[2] ferromagnetic phase transitions have been determined at temperatures below 15 K.[3] On the contrary, the compounds $\{[N(n\text{-}C_4H_9)_4][M^{II}Fe^{III}(ox)_3]\}_n$, M^{II} = Fe, Ni, behave as ferrimagnets at temperatures below 43 K and 28 K, respectively.[4] The mixed-valency compounds $\{[XR_4][Fe^{II}Fe^{III}(ox)_3]\}_n$ (X = N, P; R = *n*-propyl, *n*-butyl, phenyl) exhibit ferrimagnetism with an unprecedented anomalous negative magnetization in the tetrabutylammonium derivative.[5] Moreover, a further type with a mixed-valency network stoichiometry, $\{[A][Cr^{II}Cr^{III}(ox)_3]\}_n$ [A = $N(n\text{-butyl})_4$, $P(phenyl)_4$], shows only short-range antiferromagnetic correlations but no long-range ordering above the experimental temperature limit of 2 K.[6] Finally, $\{[N(n\text{-}C_4H_9)_4][Mn^{II}Fe^{III}(ox)_3]\}_n$ is an example revealing an antiferromagnetic transition around 50 K.[7] Recently, a crossover from ferromagnetic ordering to ferrimagnetic ordering has been shown to occur in the series $\{[N(n\text{-}C_4H_9)_4][Fe^{II}Fe_x^{III}Cr_{1-x}^{III}(ox)_3]\}_n$ as a function of the concentration parameter *x*, and particularly below the magnetic transition temperature, a spin-glass-like behavior has been determined for $x > 0.4$.[8]

* To whom correspondence should be addressed.
[†] Universität Zürich.
[‡] Eidgenössische Technische Hochschule Zürich & Paul Scherrer Institut.
[§] Hahn-Meitner-Institut, Abteilung für Neutronenstreuung.
[||] Institut Laue-Langevin.
[⊗] Abstract published in *Advance ACS Abstracts,* April 15, 1997.

(1) *Proceedings of the IV International Conference on Molecule-Based Magnets*; Molecular Crystals and Liquid Crystals; Miller, J. S., Epstein, A. J., Eds.; Gordon & Breach: London, 1995; Vols. 271−274.
(2) Decurtins, S.; Schmalle, H. W.; Oswald, H. R.; Linden, A.; Ensling, J.; Gütlich, P.; Hauser, A. *Inorg. Chim. Acta* **1994**, *216*, 65.
(3) Tamaki, H.; Zhong, Z. J.; Matsumoto, N.; Kida, S.; Koikawa, M.; Achiwa, N.; Hashimoto, Y.; Okawa, H. *J. Am. Chem. Soc.* **1992**, *114*, 6974.
(4) Tamaki, H.; Mitsumi, M.; Nakamura, K.; Matsumoto, N.; Kida, S.; Okawa, H.; Iijima, S. *Chem. Lett.* **1992**, 1975.
(5) Mathonière, C.; Carling, S. G.; Yusheng, D.; Day, P. *J. Chem. Soc., Chem. Commun.* **1994**, 1551.
(6) Nuttall, C. J.; Bellitto, C.; Day, P. *J. Chem. Soc., Chem. Commun.* **1995**, 1513.
(7) Reiff, W. M.; Kreisz, J.; Meda, L.; Kirss, R. U. *Mol. Cryst. Liq. Cryst.* **1995**, *273*, 181.
(8) Bhattacharjee, A.; Iijima, S.; Mitzutani, F. *J. Magn. Magn. Mater.* **1996**, *153*, 235.
(9) Mathonière, C.; Nuttall, C. J.; Carling, S. G.; Day, P. *Inorg. Chem.* **1996**, *35*, 1201.
(10) Atovmyan, L. O.; Shilov, G. V.; Lyubovskaya, R. N.; Zhilyaeva, E. I.; Ovanesyan, N. S.; Pirumova, S. I.; Gusakovskaya, I. G. *JETP Lett.* **1993**, *58*, 766.
(11) Carling, S. G.; Mathonière, C.; Day, P.; Malik, K. M. A.; Coles, S. J.; Hursthouse, M. B. *J. Chem. Soc., Dalton Trans.* **1996**, 1839.

S0020-1669(96)00838-5 CCC: $14.00

In view of the astonishing diversity of magnetic phenomena generated by this structurally two-dimensional molecular framework, it has to be stressed that much of the interpretation of the magnetic results relies on structural data gained from powder samples. Although much worthwhile information has resulted from a powder X-ray study on 16 representative compounds,[9] what is missing in general are more detailed single-crystal structural data. As yet only three single-crystal structure determinations have been published, two for the $[Mn^{II}Cr^{III}(ox)_3]^-$ network stoichiometry with $[P(Ph)_4]^+$ and $[N(n\text{-}C_4H_9)_4]^+$ counterions[2,10] and one for the $\{[N(n\text{-}C_5H_{11})_4][Mn^{II}Fe^{III}(ox)_3]\}_n$ stoichiometry.[11] Notice that, in contrast, the three-dimensional (3D) homometallic and heterometallic oxalate-bridged compounds with the analogous framework stoichiometry but metal−tris(bipyridines) as templating counterions reveal a much better crystallization behavior. Consequently, more crystal structure determinations, by far, have been accomplished for the 3D compounds.[12−14]

In this report we describe the single-crystal structure analysis of two 2D compounds, namely, $\{[N(n\text{-}C_3H_7)_4][Mn^{II}Cr^{III}(C_2O_4)_3]\}_n$ (**1**) and $\{[N(n\text{-}C_4H_9)_4][Mn^{II}Fe^{III}(C_2O_4)_3]\}_n$ (**2**). In particular, the structural analysis of the former compound gives reliable structural information about the tetrapropylammonium ion in its function as a templating counterion for the layer compounds. In the case of the latter stoichiometry, especially the structural parameters of the tetrabutylammonium template are now more accurately and completely described than in the previously published report.[10]

In contrast to the large body of experimental results which has been published from magnetic susceptibility and magnetization measurements with molecular-based magnetic materials, very limited experience has been gained so far from elastic neutron scattering experiments aimed at elucidating the spin structures in the magnetically ordered state. In a previous report on the magnetic structure of a 3D oxalate-bridged manganese(II) framework compound, the possibilities of the elastic neutron scattering technique with such molecular compounds were clearly shown.[15] Now, we report the results of elastic neutron scattering experiments on a 2D oxalate-bridged bimetallic compound, namely, $\{[P(C_6D_5)_4][Mn^{II}Cr^{III}(C_2O_4)_3]\}_n$ (**3**), which exhibits a long-range ferromagnetic transition at $T_c = 6$ K.

Experimental Section

Materials. All chemicals were of reagent grade and were used as commercially obtained. Standard literature procedures were used to prepare the complexes $K_3[M^{III}(C_2O_4)_3]\cdot 3H_2O$.[16]

$\{[N(n\text{-}C_3H_7)_4][Mn^{II}Cr^{III}(C_2O_4)_3]\}_n$ (1). In accordance with the published method,[2] the compound was crystallized by slow evaporation of an equimolar (15 mM) aqueous solution of the components $K_3[Cr^{III}(C_2O_4)_3]\cdot 3H_2O$, $MnCl_2\cdot 4H_2O$, and $[N(n\text{-}C_3H_7)_4]I$. The crystals show a distinct red-blue dichroism when examined under polarized light. An X-ray structural analysis was completed. Anal. Calcd for $C_{18}H_{28}CrMnNO_{12}$: C, 38.80; H, 5.06; N, 2.51; Cr, 9.33; Mn, 9.86. Found: C, 39.20; H, 4.80; N, 2.45; Cr, 8.70; Mn, 10.20.

$\{[N(n\text{-}C_4H_9)_4][Mn^{II}Fe^{III}(C_2O_4)_3]\}_n$ (2). In accordance with the published method,[2] the compound was crystallized, protected from light, by slow evaporation of an equimolar (10 mM) aqueous solution of the components $K_3[Fe^{III}(C_2O_4)_3]\cdot 3H_2O$, $MnCl_2\cdot 4H_2O$, and $[N(n\text{-}C_4H_9)_4]Cl$. The crystals show a distinct light-yellow to dark-yellow dichroism when examined under polarized light. An X-ray structural analysis was completed. Anal. Calcd for $C_{22}H_{36}FeMnNO_{12}$: C, 42.81; H, 5.88; N, 2.27; Fe, 9.05; Mn, 8.90. Found: C, 42.55; H, 6.00; N, 2.10; Fe, 8.75; Mn, 9.10.

Table 1. Crystallographic Data for Complexes **1** and **2**[a]

	1	**2**
formula	$C_{18}H_{28}CrMnNO_{12}$	$C_{22}H_{36}FeMnNO_{12}$
fw	557.35	617.31
space group	*R*3*c* (No. 161)	*P*6$_3$ (No. 173)
a, Å	9.363(3)	9.482(2)
b, Å	9.363(3)	9.482(2)
c, Å	49.207(27)	17.827(8)
V, Å^3	3736(3)	1388.1(7)
Z	6	2
T, K	295	295
calcd density, g cm^{-3}	1.486	1.477
λ(Mo Kα), Å	0.710 73	0.710 73
μ, cm^{-1}	10.01	10.37
final R and R_w indices based on F and F^2, $I > 2\sigma(I)$	0.068, 0.162	0.071, 0.185
final R and R_w indices based on F and F^2, all data	0.214, 0.255	0.153, 0.245

[a] R_1 factor definition: $R = \sum(||F_o| - |F_c||)/\sum|F_o|$. SHELXL-93 R_w factor definition: $R_w = [\sum w(F_o^2 - F_c^2)^2/\sum w(F_o^2)^2]^{1/2}$. Weighting scheme: $w = 1/[\sigma^2(F_o)^2 + (np)^2 + 0.00p]$, $p = (\max(F_o^2) + 2F_c^2)/3$.

$\{[P(C_6D_5)_4][Mn^{II}Cr^{III}(C_2O_4)_3]\}_n$ (3). $[P(C_6D_5)_4]Br$ was synthesized from deuteriobromobenzene (99% D) according to a published procedure.[17] The bromine salt was directly isolated and used without further purification. ^{1}H- and ^{2}H-NMR analysis showed a pure product with deuterium incorporation greater than 98%. The polycrystalline compound **3** was synthesized in nearly quantitative yield by stirring of a methanolic solution of $[P(C_6D_5)_4]Br$ (50 mM) with aqueous solutions (100 mM) of $K_3[Cr^{III}C_2O_4)_3]\cdot 3H_2O$ and $MnCl_2\cdot 4H_2O$. The green polycrystalline product was filtered off, washed with water and methanol, and dried in vacuo. Overall, the X-ray powder diffraction data showed the compound to be structurally isomorphous to the undeuterated reference compound.[2] Anal. Calcd for $C_{30}D_{20}CrMnO_{12}P$: C, 49.33; D, 5.51; Cr, 7.12; Mn, 7.52. Found: C, 49.80; D, 5.80; Cr, 7.00; Mn, 7.70.

Crystallographic Structure Determination. Some relevant crystallographic data and structure determination parameters for compounds **1** and **2** are given in Table 1. Unit cell parameters were determined and intensity data were collected by using an Enraf-Nonius CAD-4 diffractometer with graphite-monochromatized Mo Kα radiation. For the purpose of checking the crystal stability, three standard reflections were monitored at intervals of every 3 h for **1** and **2**. The variation of standards was between 1.1% and 2.4%. Orientation control was performed by measuring three standard reflections every 400 reflections. Intensities were corrected for Lorentz and polarization effects, and numerical absorption corrections based on seven (**1**) and 13 (**2**) crystal faces were applied.

A red-blue dichroitic, irregularly shaped platelet crystal of **1** with approximate dimensions of $0.44 \times 0.43 \times 0.15$ mm^3 was selected for the X-ray experiment. A triclinic cell with $a = 9.355(4)$ Å, $b = 9.371(2)$ Å, $c = 17.276(9)$ Å, $\alpha = 90.07(3)°$, $\beta = 105.75(4)°$, $\gamma = 119.94(3)°$, and $V = 1246(1)$ Å^3 was determined by least-squares refinement of the θ angles of 25 reflections in the interval $5.7° < \theta < 11.9°$. The number of intensity data collected was 6401 (including 60 standards). The corrected data were transformed by a matrix ($-1\ 0\ 0$, $1\ 1\ 0$, $-2\ -1\ -3$), calculated with the LEPAGE program,[18] resulting in the possible space groups $R\bar{3}c$ and $R3c$, in accordance with systematic extinction rules for hexagonal settings. In analogy to the rhombohedric structure which crystallizes with $[P(C_6H_5)_4]^+$ cations, the polar space group $R3c$ was chosen.[2] The new cell dimensions are shown in Table 1. After merging, 2546 unique reflections remained in space group $R3c$ ($R_{int} = 0.137$). The structure was solved by using a combination

(12) Decurtins, S.; Schmalle, H. W.; Schneuwly, P.; Ensling, J.; Gütlich, P. *J. Am. Chem. Soc.* **1994**, *116*, 9521.
(13) Decurtins, S.; Schmalle, H. W.; Pellaux, R.; Schneuwly, P.; Hauser, A. *Inorg. Chem.* **1996**, *35*, 1451.
(14) Schmalle, H. W.; Pellaux, R.; Decurtins, S. *Z. Kristallogr.* **1996**, *211*, 533.
(15) Decurtins, S.; Schmalle, H. W.; Pellaux, R.; Huber, R.; Fischer, P.; Ouladdiaf, B. *Adv. Mater.* **1996**, *8*, 647.
(16) Bailar, J. C.; Jones, E. M. In *Inorganic Synthesis*; Booth, H. S., Ed.; McGraw-Hill: New York, 1939; Vol. 1, p 35.
(17) Willard, H. H.; Perkins, L. R.; Blicke, F. F. *J. Am. Chem. Soc.* **1948**, *70*, 737.
(18) LePage, Y. *J. Appl. Crystallogr.* **1982**, *15*, 255.

of the Patterson interpretation routine in SHELXS-86[19] and difference Fourier calculations during refinement on F^2 with SHELXL-93.[20] The anionic 2D MnCr−oxalate network could be assigned without difficulties and refined anisotropically; however, the tetrapropylammonium cation had to be refined with 19 restraints, using a model from the literature.[21] All hydrogen atomic positions were calculated and refined as a riding model.

A dichroitic, yellow-colored crystal of **2** showing an irregular hexagonal prismatic morphology with approximate dimensions of 0.37 × 0.28 × 0.20 mm^3 was used for the X-ray structure determination. A hexagonal unit cell was determined from 25 indexed reflections (range $6.9° < \theta < 15.1°$). The number of intensity data measured was 4442 (including 45 standards), and the usual corrections (as for **1**) were applied. After merging, 1395 unique reflections remained (R_{int} = 0.087). The structure was solved in space group $P6_3$ using the same programs and procedures as for compound **1**. The anionic 2D MnFe−oxalate network was refined anisotropically, while the heavily disordered tetrabutylammonium cation was refined isotropically with 36 intrachain distance restraints. Two different chain conformations could be assigned. The hydrogen atomic positions for these conformations were calculated separately by using the PART instructions in SHELXL-93[20] and refined as a riding model.

Magnetic Measurements. Magnetic susceptibility data of the polycrystalline compounds **1** and **2** and single-crystal magnetization data of compound **1** were collected with a Quantum Design SQUID susceptometer. The polycrystalline samples were measured in a quartz tube in the temperature range 300−4 K at a field of 100 G, whereas the single crystal of **1** was mounted on the top of a quartz rod and the magnetization data were recorded at 4.2 K in the field range 10−6000 G parallel and perpendicular to the *c*-axis. Diamagnetic corrections for the constituting atoms were made using Pascal's constants.

Neutron Diffraction. Neutron diffraction experiments for refinement of the structural parameters of compound **3** were performed on the D2B diffractometer at the high-flux reactor of the Institut Laue-Langevin (ILL) in Grenoble at the temperatures 1.8, 20, and 295 K. Experimental details: high-intensity mode with neutron wavelength λ = 2.398 Å; due to the absence of a graphite filter, some contamination from $\lambda/2$ was present; 2θ scans in the range 5.0−160.0° were performed; refinements were based on the X-ray structure determination[2] in space groups *R*3*c* and *R*32 and were carried out using the structure profile refinement program FullProf in the profile matching mode.[22,23] Two lattice parameters and six line-profile parameters were varied.

Neutron diffraction experiments for establishing the magnetic structure were performed on the V1 diffractometer at the cold neutron source of the reactor of the Hahn-Meitner-Institut (HMI) in Berlin in the temperature range 1.8−12 K. Experimental details: neutron wavelength λ = 4.766 Å; a beryllium filter was used to avoid contamination with $\lambda/2$; 2θ scans in the range 10.00−109.75°, as well as temperature dependent measurements of the dominant magnetic reflection with a fixed detector position were performed; calculations were carried out using the structure profile refinement program FullProf;[22,23] the difference diffraction pattern I(1.8 K) − I(12 K) was treated as a pure magnetic phase; calculations were based on the cell parameters and metal positions of the corresponding single-crystal X-ray structure determination in space group *R*3*c*; the magnetic moments were fixed to the values 5 μ_B for Mn^{2+} and 3 μ_B for Cr^{3+}.

Results and Discussion

Description of the Structures {[N(*n*-C_3H_7)$_4$][$Mn^{II}Cr^{III}$(C_2O_4)$_3$]}$_n$ (1) and {[N(*n*-C_4H_9)$_4$][$Mn^{II}Fe^{III}$(C_2O_4)$_3$]}$_n$ (2). The crystal structures of both compounds consist of bimetallic, anionic two-dimensional networks with stoichiometry [$Mn^{II}M^{III}(C_2O_4)_3]_n^{n-}$, which are interleaved by layers formed through the templating counterions. Thus, the general structural features

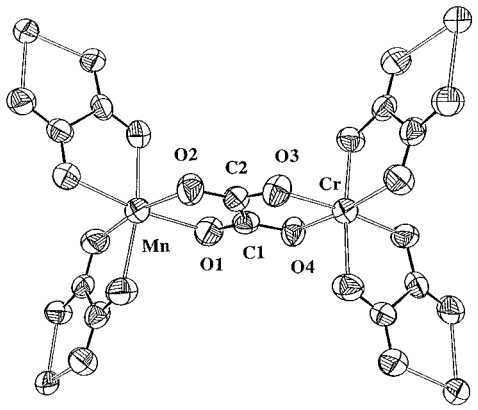

Figure 1. ORTEP drawing (50% probability level) with the labeling scheme of the Mn and Cr coordination of the compound {[N(*n*-C_3H_7)$_4$][$Mn^{II}Cr^{III}$(C_2O_4)$_3$]}$_n$ (**1**).

Table 2. Fractional Coordinates (×10^4) and Equivalent Isotropic Displacement Parameters (Å^2 × 10^3) for **1**

	x	*y*	*z*	$U_{(eq)}$[a]/$U_{(iso)}$[b]
Mn	6667	3333	9972(1)	52(1)
Cr	13333	6667	9954(1)	44(1)
O(1)	8742(6)	5194(6)	10193(1)	59(2)
O(2)	8735(6)	3579(6)	9738(1)	59(2)
O(3)	11462(5)	4976(6)	9735(1)	52(2)
O(4)	11531(6)	6588(5)	10179(1)	48(1)
C(1)	10087(8)	5518(7)	10092(2)	41(2)
C(2)	10094(9)	4597(8)	9827(2)	47(2)
N(1)	10000	10000	9337(2)	68(3)
C(11)	9415(15)	8236(7)	9211(2)	257(9)
C(21)	10312(14)	7350(10)	9234(4)	200(10)
C(31)	9529(23)	5614(14)	9132(4)	206(6)
C(12)	10015(25)	10148(22)	9636(2)	190(17)[b]
C(22)	10186(33)	9154(29)	9855(2)	108(11)[b]
C(32)	9705(41)	9501(25)	10131(3)	81(9)

[a] $U_{(eq)}$ is defined as one-third of the trace of the orthogonalized U_{ij} tensor. [b] Isotropically refined atoms.

are very much comparable to those which have already been reported for the compound {[$P(C_6H_5)_4$][$Mn^{II}Cr^{III}$(C_2O_4)$_3$]}$_n$ and similar to the recently published data for the compound {[N(*n*-C_5H_{11})$_4$] [$Mn^{II}Fe^{III}$(C_2O_4)$_3$]}$_n$.[2,11]

Structure 1. Figure 1 shows an ORTEP drawing of the manganese and chromium coordinations of the zero layer of the unit cell for compound **1**. Within space group *R*3*c* (hexagonal setting), the unit cell has been determined to be built up by six anionic and cationic layers, and consequently, a rather large *c*-axis of 49.207(27) Å results. Tables 2 and 3 summarize the atomic fractional coordinates and selected bond lengths and angles for **1**. The geometric values of the metal coordination spheres and of the bridging oxalate ligands compare well with those described for the analogous compound with the same network stoichiometry but $[P(C_6H_5)_4]^+$ cations.[2] Both types of metal ions are lying on special sites with a 3-fold axis (Wyckoff letter a); thus, within an anionic layer, a regular hexagonal pattern results. In contrast, for the compound where the $[P(C_6H_5)_4]^+$ cations form the interleaving layers, slightly elongated ellipsoids of the connected nets occur and, consequently, the *a*-axis within *R*3*c* amounts to a double value of 18.783(3) Å. Figure 2, a [001] projection, exhibits an overall view of an anionic and cationic layer, whereby the alternating chirality of neighboring [$M(C_2O_4)_3$] subunits can be readily seen. Figure 3, a [110] projection of the unit cell, depicts the regular arrangement of the interleaving [N(*n*-C_3H_7)$_4$]$^+$ cations. One of the propyl chains points vertically to the anionic layers while fitting exactly into the center of a vacancy, and the remaining three propyl chains extend into the interlayer spacing. All four

(19) Sheldrick, G. M. *Acta Crystallogr.* **1990**, *A46*, 467.
(20) Sheldrick, G. M. *Program for Crystal Structure Refinement*; University of Göttingen: Göttingen, Germany, 1993.
(21) Yoshida, T.; Nagata, K.; Yasuniwa, M.; Yoshimatsu, M.; Wunderlich, B. *Acta Crystallogr.* **1994**, *C50*, 1758.
(22) Wiles, D. B.; Young, R. A. *J. Appl. Crystallogr.* **1981**, *14*, 149.
(23) Rodriguez, J. *Physica* **1993**, *B192*, 55.

Table 3. Selected Bond Lengths (Å) and Angles (deg) for **1**[a]

Distances			
Mn−O(1)	2.147(5) 3*x*		
Mn−O(2)	2.164(6) 3*x*	N(1)−C(12)	1.477(10)
Cr−O(4)	1.989(5) 3*x*	N(1)−C(11)	1.584(6) 3*x*
Cr−O(3)	1.990(5) 3*x*		
		C(1)−C(2)	1.564(8)
O(1)−C(1)	1.242(8)	C(11)−C(21)	1.450(11) 3*x*
O(2)−C(2)	1.228(8)	C(21)−C(31)	1.497(11) 3*x*
O(3)−C(2)	1.231(9)	C(12)−C(22)	1.487(13)
O(4)−C(1)	1.289(8)	C(22)−C(32)	1.516(14)

Angles			
O(1)^{i}−Mn−O(1)	96.6(2) 3*x*	O(1)−C(1)−O(4)	126.8(7)
O(1)−Mn−O(2)^{i}	169.9(2) 3*x*	O(1)−C(1)−C(2)	118.8(5)
O(1)^{i}−Mn−O(2)	92.3(2) 3*x*	O(4)−C(1)−C(2)	114.4(5)
O(1)−Mn−O(2)	77.6(2) 3*x*	O(2)−C(2)−O(3)	128.1(8)
O(2)−Mn−O(2)^{ii}	94.3(2) 3*x*	O(2)−C(2)−C(1)	116.0(7)
O(4)−Cr−O(4)^{iii}	92.0(2) 3*x*	O(3)−C(2)−C(1)	115.9(5)
O(4)−Cr−O(3)^{iv}	173.8(2) 3*x*	C(12)−N(1)−C(11)	118.1(9)
O(4)−Cr−O(3)^{iii}	91.8(2) 3*x*	C(12)^{v}−N(1)−C(11)	109.5(10)
O(4)−Cr−O(3)	83.0(2) 3*x*	C(12)^{vi}−N(1)−C(11)	111.5(9)
O(3)^{iv}−Cr−O(3)	93.5(2) 3*x*	C(11)−N(1)−C(11)^{vi}	105.6(5)
C(1)−O(1)−Mn	113.0(5)	C(21)−C(11)−N(1)	124.7(9)
C(2)−O(2)−Mn	114.6(6)	C(11)−C(21)−C(31)	119.1(12)
C(2)−O(3)−Cr	113.9(5)	N(1)−C(12)−C(22)	131.6(14)
C(1)−O(4)−Cr	112.6(5)	C(12)−C(22)−C(32)	112(2)

[a] Symmetry transformations used to generate equivalent atoms: (i) $-x + y + 1, -x + 1, z$; (ii) $-y + 1, x-y, z$; (iii) $-x + y + 2, -x + 2, z$; (iv) $-y + 2, x-y, z$; (v) $-y + 2, x-y + 1, z$; (vi) $-x + y + 1, -x + 2, z$.

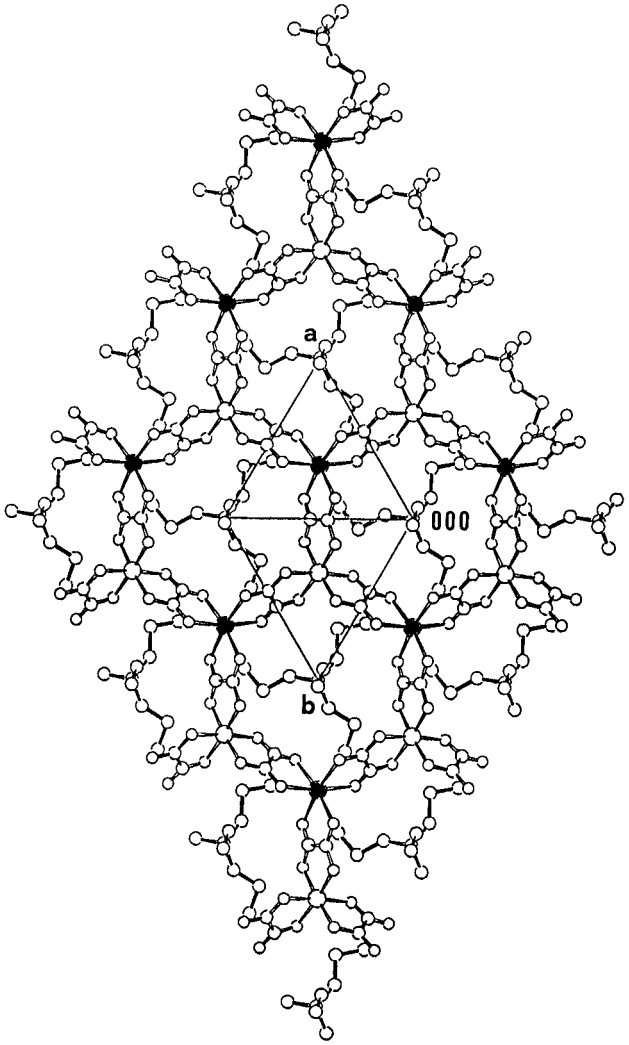

Figure 2. SCHAKAL drawing, [001] projection, of a sector from the $[Mn^{II}Cr^{III}(C_2O_4)_3]_n^{n-}$ layer of compound **1** including one adjacent cationic layer. Black atoms indicate Mn positions.

Table 4. Fractional Coordinates ($\times 10^4$) and Equivalent Isotropic Displacement Parameters (Å^2 $\times$ 10^3) for **2**

	x	*y*	*z*	$U_{(eq)}$[a]/$U_{(iso)}$[b]
Fe	6667	3333	4115(2)	60(1)
Mn	10000	0	4108(1)	61(1)
O(1)	8300(6)	3046(6)	4789(3)	65(2)
O(2)	8202(6)	221(6)	3508(3)	69(2)
O(3)	6884(6)	1600(6)	3515(3)	65(2)
O(4)	9721(6)	1713(7)	4780(3)	73(2)
C(1)	8716(7)	2093(9)	4501(4)	56(2)
C(2)	7856(8)	1236(8)	3766(5)	56(2)
N(1)	6667	3333	7208(4)	91(4)[b]
C(11A)	6252(15)	1648(6)	6867(6)	287(20)[b]
C(11B)	7130(9)	2081(7)	6881(6)	185(22)[b]
C(21A)	6232(14)	257(8)	7230(9)	339(32)[b]
C(21B)	6756(15)	531(9)	7293(9)	215(28)[b]
C(31A)	7143(16)	−434(16)	6763(12)	206(13)[b]
C(31B)	5947(16)	−978(14)	6779(14)	148(15)[b]
C(41A)	5997(33)	−1777(25)	6228(14)	288(23)[b]
C(41B)	7137(22)	−1586(27)	6596(27)	259(36)[b]
C(12)	6735(14)	3322(17)	8048(4)	297(32)[b]
C(22)	5706(19)	3452(33)	8647(6)	112(11)[b]
C(32)	6483(25)	3892(29)	9448(8)	118(13)[b]
C(42)	6984(57)	3155(67)	10097(30)	496(77)[b]

[a] $U_{(eq)}$ is defined as one-third of the trace of the orthogonalized U_{ij} tensor. [b] Isotropically refined atoms.

chains are found to be in fully extended conformations. The nitrogen atoms are located on special sites with a 3-fold axis (Wyckoff letter a). But it has to be noted that in Figures 2 and 3, for reasons of clarity, the axial propyl chains show only one of the three equivalent positions which are statistically occupied. Whereas, in the case of the interleaving $[P(C_6H_5)_4]^+$ cations,[2] the interlayer separation of the anionic networks amounts to 9.55 Å, the $[N(n\text{-}C_3H_7)_4]^+$ cations cause, as expected, a smaller interlayer distance of 8.20 Å.

Structure 2. An ORTEP drawing of the manganese and iron coordinations of the zero layer of the unit cell for compound **2** is shown in Figure 4. Within space group $P6_3$, for symmetry reasons, only two anionic and cationic layers build up the unit cell, and correspondingly, a shorter *c*-axis of 17.827(8) Å results. Tables 4 and 5 summarize the atomic fractional coordinates and selected bond lengths and angles for **2**. Whereas the geometric parameters of the bridging oxalate ligands compare well with those described for the analogous compound with the same network stoichiometry, but $[N(n\text{-}C_5H_{11})_4]^+$ cations,[11] the metal to oxygen distances deviate in a significant manner from those of that compound. At the manganese(II) site, the mean metal to oxygen distance is 2.124(6) Å, and at the iron(III) site, it is 2.069(6) Å, whereas for the cited compound[11] the mean Mn(II)−O distance [2.092(6) Å] is found to be smaller than the mean Fe(III)−O distance [2.111(6) Å]. For comparison, further examples of mean Mn(II)−O distances are, e.g., 2.156(6) Å for compound **1**, 2.13(2) Å for the compound analogous to **1** but with $[P(Ph)_4]^+$ cations,[2] and 2.154(2) and 2.166(2) Å for a three-dimensionally linked manganese(II) oxalato compound.[12] In addition, a mean Fe(III)−O distance of 1.994(2) Å was determined in the case of a three-dimensionally connected iron(III) oxalato complex.[12] Obviously, the packing of the organic cations, as exemplified with $[N(n\text{-}C_5H_{11})_4]^+$ counterions, influences the metal−oxygen bond lengths to a considerable extent.

Notice that, as with compound **1**, both types of metal ions are lying on special sites with a 3-fold axis [Wyckoff letters a (Mn) and b (Fe)]; thus, within an anionic layer, a regular honeycomb pattern results. Figure 5 displays a [001] projection of an anionic network together with one cation of the adjacent layer. The nitrogen atoms are also located on special sites with a 3-fold axis (Wyckoff letter b). As can be readily seen, the

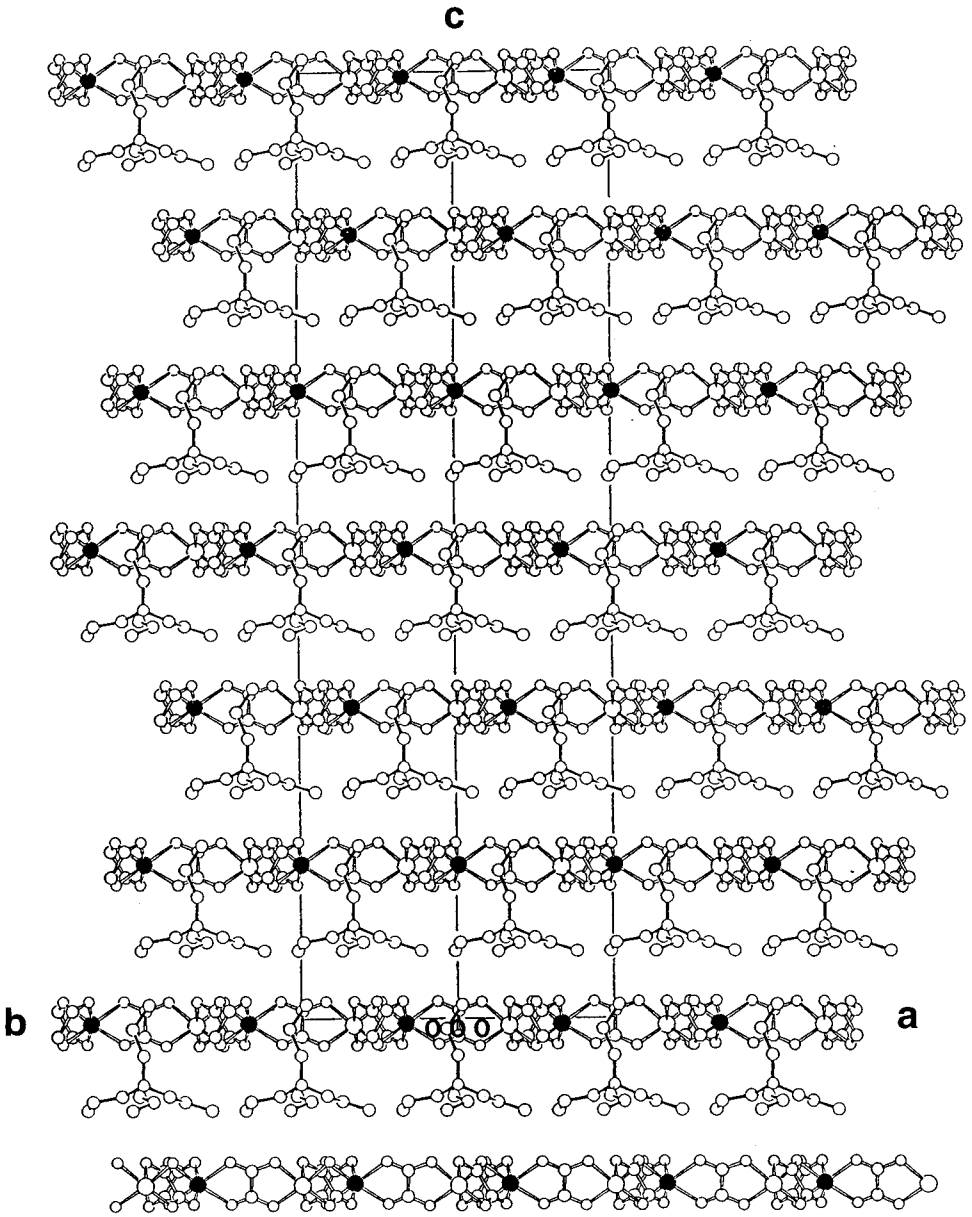

Figure 3. [110] projection of $\{[N(n\text{-}C_3H_7)_4][Mn^{II}Cr^{III}(C_2O_4)_3]\}_n$ (**1**). Black atoms indicate Mn positions.

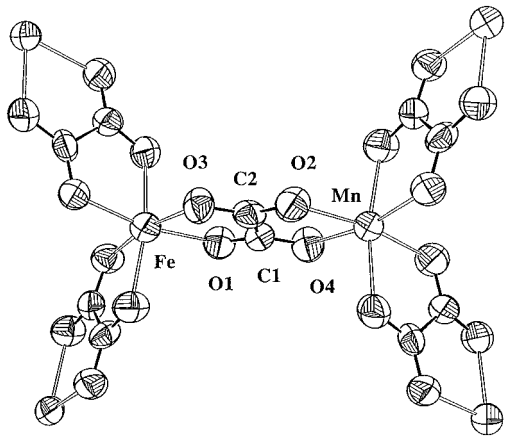

Figure 4. ORTEP drawing (50% probability level) with the labeling scheme of the Mn and Fe coordination of the compound $\{[N(n\text{-}C_4H_9)_4][Mn^{II}Fe^{III}(C_2O_4)_3]\}_n$ (**2**).

axial butyl chains point vertically in fully extended conformations into the voids of the anionic nets, but for the sake of pictorial clarity, for each chain, only one of the three equivalent positions is shown. The equatorial butyl chains exhibit a conformational variability in that two different conformations have been found to occur. They have been designated with C(A) and C(B) in Tables 4 and 5. Figure 6, a [100] projection, depicts both conformations of the equatorial butyl chains which have been refined in a ratio of approximately 2:1 for molecules A and B. By comparison to structure **1** with tetrapropylammonium cations, the tetrabutylammonium cations give rise to an increase of the interlayer separation of the anionic networks of 0.71 Å to a value of 8.91 Å.

Magnetic Properties. Previous magnetic susceptibility and magnetization studies of polycrystalline $\{[A][Mn^{II}Cr^{III}(C_2O_4)_3]\}_n$ network compounds revealed a ferromagnetic ordering behavior at $T_c = 6$ K.[2,3] It was on this basis and because of the availability of single crystals of **1** that a further magnetization experiment was undertaken with the aim of revealing the degree of magnetic anisotropy occurring in these structurally two-dimensional compounds. Figure 7 shows the result of the field dependent magnetization measurement at $T = 4.2$ K with a single crystal of **1**. The applied magnetic field was directed either parallel or perpendicular to the crystallographic *c*-axis. Obviously, the system expresses a large anisotropy such that the easy axis of magnetization is lying predominantly in the

Table 5. Selected Bond Lengths (Å) and Angles (deg) for **2**[a]

Distances			
Fe−O(3)	2.056(6) 3*x*	N(1)−C(11B)	1.570(6)
Fe−O(1)	2.082(6) 3*x*		
Mn−O(2)	2.110(6) 3*x*	C(1)−C(2)	1.543(9)
Mn−O(4)	2.138(6) 3*x*	C(11A)−C(21A)	1.462(11)
		C(11B)−C(21B)	1.518(10)
O(1)−C(1)	1.261(9)	C(21A)−C(31A)	1.560(13)
O(2)−C(2)	1.250(9)	C(21B)−C(31B)	1.542(13)
O(3)−C(2)	1.219(9)	C(31A)−C(41A)	1.526(14)
O(4)−C(1)	1.277(9)	C(31B)−C(41B)	1.537(14)
		C(12)−C(22)	1.492(13)
N(1)−C(12)	1.500(9)	C(22)−C(32)	1.564(13)
N(1)−C(11A)	1.565(6)	C(32)−C(42)	1.544(16)

Angles			
O(3)^{i}−Fe−O(3)	95.4(2) 3*x*	O(3)−C(2)−O(2)	127.5(7)
O(3)^{i}−Fe−O(1)	96.0(2) 3*x*	O(3)−C(2)−C(1)	116.0(6)
O(3)^{ii}−Fe−O(1)	167.8(2) 3*x*	O(2)−C(2)−C(1)	116.5(7)
O(3)−Fe−O(1)	79.5(2) 3*x*	C(12)−N(1)−C(11A)	111.8(7)
O(1)−Fe−O(1)^{i}	90.1(2) 3*x*	C(12)^{ii}−N(1)−C(11A)	111.3(6)
O(2)^{iii}−Mn−O(2)	96.5(2) 3*x*	C(12)^{i}−N(1)−C(11A)	115.5(7)
O(2)^{iv}−Mn−O(4)	94.4(2) 3*x*	C(11A)−N(1)−C(11A)^{i}	105.9(5)
O(2)^{iii}−Mn−O(4)	168.3(2) 3*x*	C(11B)−N(1)−C(11B)^{i}	107.0(5)
O(2)−Mn−O(4)	78.2(2) 3*x*	C(21A)−C(11A)−N(1)	129.3(9)
O(4)−Mn−O(4)^{iii}	91.7(2) 3*x*	C(21B)−C(11B)−N(1)	122.2(8)
C(1)−O(1)−Fe	112.3(5)	C(11A)−C(21A)−C(31A)	112.5(11)
C(2)−O(2)−Mn	115.2(5)	C(11B)−C(21B)−C(31B)	112.2(12)
C(2)−O(3)−Fe	115.3(5)	C(41A)−C(31A)−C(21A)	111.8(13)
C(1)−O(4)−Mn	113.0(5)	C(41B)−C(31B)−C(21B)	111.0(13)
O(1)−C(1)−O(4)	126.2(7)	C(22)−C(12)−N(1)	133.0(11)
O(1)−C(1)−C(2)	116.8(6)	C(12)−C(22)−C(32)	116(2)
O(4)−C(1)−C(2)	117.0(7)	C(42)−C(32)−C(22)	141(3)

[a] Symmetry transformations used to generate equivalent atoms: (i) $-y+1, x-y, z$; (ii) $-x+y+1, -x+1, z$; (iii) $-y+1, x-y-1, z$; (iv) $-x+y+2, -x+1, z$

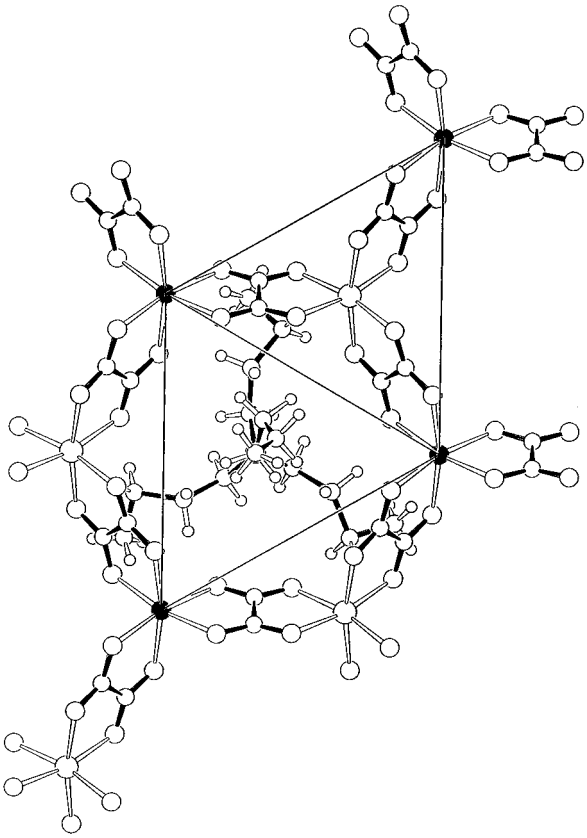

Figure 5. [001] projection of a sector from the $[Mn^{II}Fe^{III}(C_2O_4)_3]_n^{n-}$ layer of compound **2** including one adjacent cation.

direction of the *c*-axis. In this parallel orientation, a saturation is reached in a field ≈0.1 T, while the saturation field in the perpendicular direction is >0.3 T. These findings are in accordance with a previous study on the tetrabutylammonium derivative[24] and with the interpretation of the neutron scattering results of compound **3** (vide infra).

A magnetic susceptibility measurement of a polycrystalline sample of compound **2** exhibits a broad maximum near 55 K, in accordance with the reported results in refs 7 and 9, where this behavior is interpreted as corresponding to low-dimensional antiferromagnetism. Consequently, a single-crystal magnetization measurement, as was carried out for compound **1**, is not possible with the antiferromagnet **2**.

Neutron Scattering Results. On the basis of the results of magnetic susceptibility and magnetization studies of the ferromagnetic microcrystalline compounds $\{[A][Mn^{II}Cr^{III}(C_2O_4)_3]\}_n$[2,3,10] and of the ferromagnetic single crystal of compound **1**, elastic neutron scattering experiments were undertaken with the goal of revealing the magnetic structure of the ferromagnetic phase (T_c = 6 K) of this specific $Mn^{II}Cr^{III}$ network stoichiometry. Thereby, a polycrystalline sample of compound **3** was chosen as a deuterated target compound. First, the structural part of the neutron diffraction pattern of compound **3** had to be examined in the liquid-helium temperature range. Figure 8 shows a profile matching of the 1.8 K D2B neutron diffraction pattern of a polycrystalline sample of **3**. The refined unit cell parameters in space group *R*3*c* at *T* = 1.8 K have the values *a* = *b* = 18.750(9) Å, *c* = 56.01(4) Å. Overall, they are in good agreement with those parameters which were determined by the room-temperature single-crystal X-ray measurement of the undeuterated compound [*a* = *b* = 18.783(3) Å, *c* = 57.283(24) Å].[2] However, as a matter of fact, this neutron diffraction pattern at 1.8 K clearly shows that some reflections at low 2θ angles cannot be explained with these refined unit cell parameters in *R*3*c*. Therefore, an X-ray remeasurement of the same single crystal which was used in the former room-temperature X-ray study[2] was undertaken at 150 K. From that measurement, the observation of additional reflections led to the unit cell parameters *a* = *b* =18.792(10) Å, *c* = 113.43(16) Å, hence to a doubling of the *c*-axis. This doubling of the *c*-axis destroys systematic extinction rules for space group *R*3*c*. Consequently, space group *R*32 could be possible, but that means that four symmetry independent anionic and cationic layers would have to be found in the difference map, which was not possible up to now, considering the number of observed data [7436 > 2σ(*I*)].

Nevertheless, the profile matching of the 1.8 K neutron diffraction pattern of a polycrystalline sample of **3** based on the doubling of the *c*-axis within *R*32, as shown in Figure 9, reveals now a nearly featureless difference diffraction plot. The refined unit cell parameters show the values *a* = *b* = 18.749(3) Å, *c* = 111.89(3) Å. The data of the 20 and 295 K neutron diffraction experiments did not show satisfactory statistics in order to gain a reliable refinement for the unit cell parameters. Clearly, further detailed crystallographic studies at low temperatures have to be started in order to reveal the exact nature of this superstructure in *R*3*c*.

Furthermore, as anticipated from the magnetic susceptibility data, a difference in the peak intensities due to long-range ferromagnetic ordering of the magnetic moments from the Mn^{2+} and Cr^{3+} ions could be detected from the neutron diffraction experiment performed at the V1 diffractometer at the temperatures 1.8 and 12 K. Figure 10 illustrates the observed [difference *I*(1.8 K) − *I*(12 K)] and calculated magnetic neutron diffraction patterns. The temperature dependence of the dominant magnetic intensity at 2θ = 69.1° indicates an ordering

(24) Ovanesyan, N. S.; Shilov, G. V.; Atovmyan, L. O.; Lyubovskaya, R. N.; Pyalling, A. A. *Mol. Cryst. Liq. Cryst.* **1995**, *273*, 175.

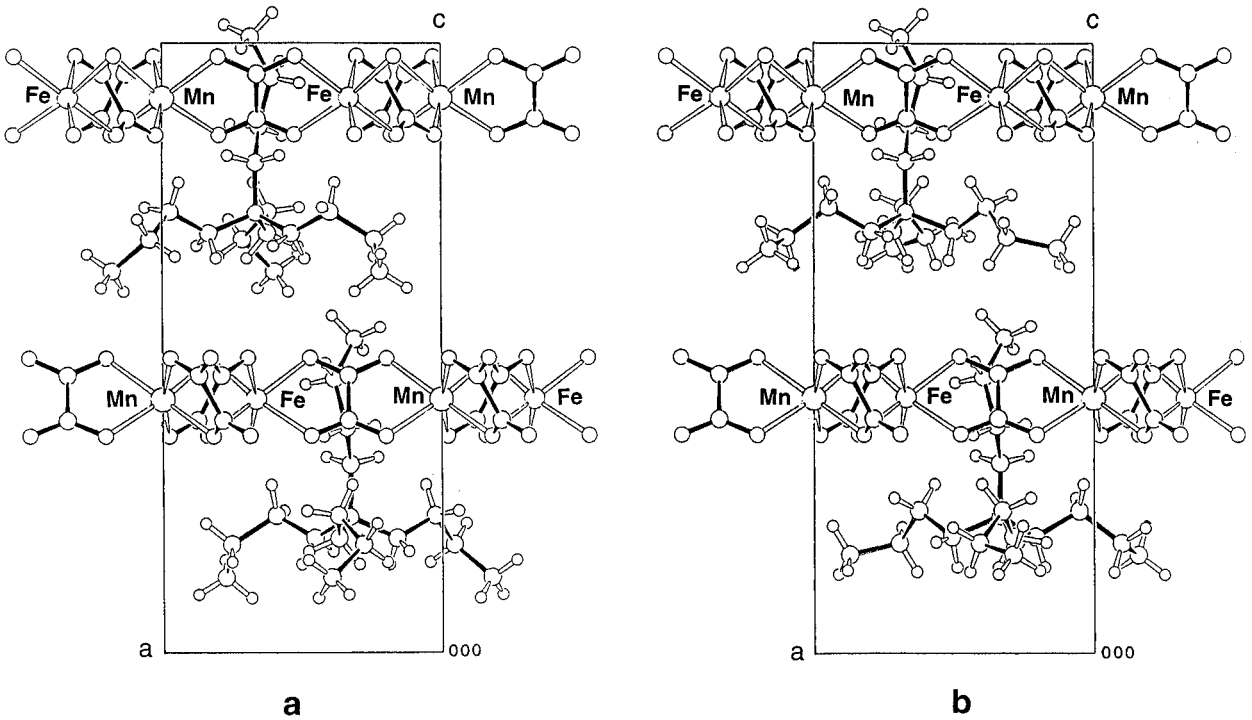

Figure 6. [100] projection of $\{[N(n\text{-}C_4H_9)_4][Mn^{II}Fe^{III}(C_2O_4)_3]\}_n$ (**2**) depicting (a) cationic conformation A and (b) cationic conformation B.

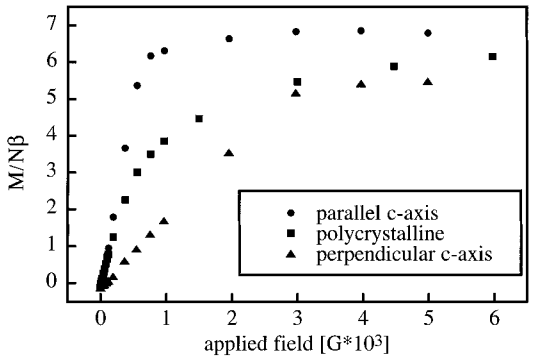

Figure 7. Plot of the field dependence of the magnetization for a single crystal of **1** at $T = 4.2$ K. The external magnetic field is applied parallel and perpendicular to the *c*-axis.

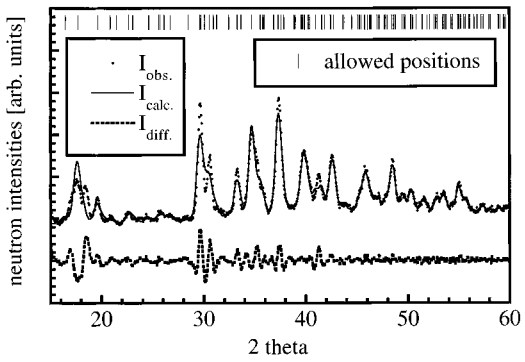

Figure 8. Observed D2B neutron diffraction pattern of a polycrystalline sample of **3** at T = 1.8 K with the profile matching plot based on a refined *c*-axis of 56.01(4) Å within space group *R*3*c*.

temperature of 6.0(5) K, in good agreement with the magnetic susceptibility experiment.[2,3] This observed enhancement in some of the Bragg reflections proves the presence of long-range magnetic interactions within this structurally two-dimensional compound. The magnetic moment configuration of the metal ions within the bimetallic layers remains to be discussed. The best agreement between observed and calculated neutron intensities was achieved with a collinear ferromagnetic arrangement of both the Mn^{2+} and Cr^{3+} spins along the *c*-axis. Thereby, the model for the calculated neutron intensities is based on a propagation vector $\mathbf{K} = 0$, because all magnetic neutron intensity peaks show an origin on a structural Bragg peak. Moreover, the structural parameters of the metal ions are taken from the structure determination in space group *R*3*c*, whereby

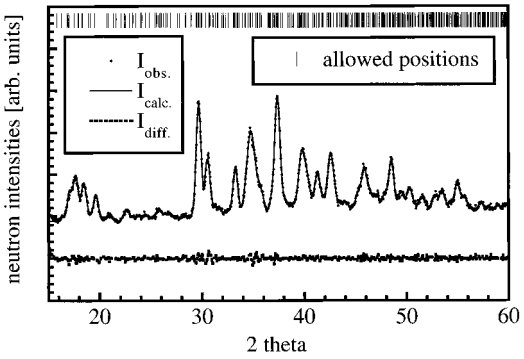

Figure 9. Observed neutron diffraction pattern as in Figure 8 but with the profile matching plot based on a refined *c*-axis of 111.97(3) Å within space group *R*32.

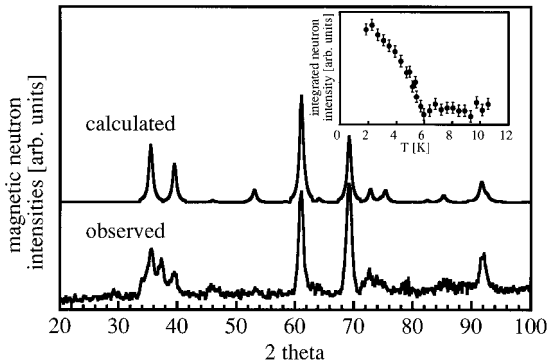

Figure 10. Observed V1 [difference $I(1.8\text{ K}) - I(12\text{ K})$] and calculated magnetic neutron diffraction patterns for compound **3**. The calculation is based on a ferromagnetic spin configuration parallel to the *c*-axis. The inset displays the temperature dependence of the integrated neutron intensity of the $2\theta = 69.1°$ peak.

it is assumed that these parameters will be the same for a possible superstructure in *R*32. Although the calculated magnetic diffraction pattern still shows some deviations from the observed data, this model with all spins parallel to the *c*-axis gives by far the best agreement. Moreover, this picture is consistent with the results of the single-crystal magnetization experiment which showed the *c*-axis to be the easy axis of magnetization. The existing differences between observed and calculated magnetic diffraction intensities are not yet understood and remain to be clarified with further experimental and theoretical studies. In particular, the exact nature of the superstructure phenomenon has to be investigated, and the corresponding study is in progress.

Concluding Remarks

With this report, two 2D polymeric structures of 3d-metal ions bridged by chelating oxalate ligands have been presented. Up to now, the structural influences of four different counterions, $A^+ = [N(n\text{-pentyl})_4]^+$, $[P(\text{phenyl})_4]^+$, $[N(n\text{-butyl})_4]^+$, and $[N(n\text{-propyl})_4]^+$, have been established by single-crystal X-ray measurements. These counterions in turn cause a decreasing interlayer separation according to the values 9.94 Å, 9.55 Å, 8.91 Å, and 8.20 Å. Clearly, the observation of the superstructure phenomenon, which is more likely to occur within the 2D systems than within the 3D compounds, calls for further and more elaborate crystallographic studies.

From a successful elastic neutron scattering experiment on the 2D manganese(II)−chromium(III) network compound, an enhancement could be observed in some of the Bragg reflections at temperatures below T_c, which corresponds to a three-dimensional, long-range magnetic ordering of the metal ion spin moments. The calculated model of the magnetic spin configuration matches fairly well the observed magnetic difference pattern. In addition, the evolution of the intensities of these magnetic Bragg reflections with temperature is in accordance with the determination of $T_c = 6$ K from the magnetic susceptibility measurements.

Further experiments which aim to reveal the magnetic structure of different 2D, bimetallic oxalate-bridged compounds are needed for obtaining information complementary to the magnetic susceptibility measurements and to gain experience with the neutron scattering technique in the case of the 2D systems. As an example, neutron scattering experiments on $[P(C_6D_5)_4][Fe^{II}Cr^{III}(C_2O_4)_3]$, where magnetic susceptibility experiments show ferromagnetic behavior analogous to that of compounds **1** and **3**, are in progress.

Acknowledgment. Gratitude is expressed to the Swiss National Science Foundation for financial support under Project No. 20-45750.95. The authors thank Dr. A. Linden, University of Zürich, for collecting a new X-ray data set at 150 K.

Supporting Information Available: Tables of atomic fractional coordinates for hydrogen atoms and anisotropic displacement parameters for **1** and **2** (5 pages). Ordering information is given on any current masthead page.

IC960838G